

Flash flood susceptibility analysis and its mapping using different bivariate models in Iran: a comparison between Shannon's entropy, statistical index, and weighting factor models

Khabat Khosravi · Hamid Reza Pourghasemi ·
Kamran Chapi · Masoumeh Bahri

Received: 2 August 2016 / Accepted: 31 October 2016 / Published online: 8 November 2016
© Springer International Publishing Switzerland 2016

Abstract Flooding is a very common worldwide natural hazard causing large-scale casualties every year; Iran is not immune to this threat as well. Comprehensive flood susceptibility mapping is very important to reduce losses of lives and properties. Thus, the aim of this study is to map susceptibility to flooding by different bivariate statistical methods including Shannon's entropy (SE), statistical index (SI), and weighting factor (Wf). In this regard, model performance evaluation is also carried out in Haraz Watershed, Mazandaran Province, Iran. In the first step, 211 flood locations were identified by the documentary sources and field inventories, of which 70% (151 positions) were used for flood susceptibility

modeling and 30% (60 positions) for evaluation and verification of the model. In the second step, ten influential factors in flooding were chosen, namely slope angle, plan curvature, altitude, topographic wetness index (TWI), stream power index (SPI), distance from river, rainfall, geology, land use, and normalized difference vegetation index (NDVI). In the next step, flood susceptibility maps were prepared by these four methods in ArcGIS. As the last step, receiver operating characteristic (ROC) curve was drawn and the area under the curve (AUC) was calculated for quantitative assessment of each model. The results showed that the best model to estimate the susceptibility to flooding in Haraz Watershed was SI model with the prediction and success rates of 99.71 and 98.72%, respectively, followed by Wf and SE models with the AUC values of 98.1 and 96.57% for the success rate, and 97.6 and 92.42% for the prediction rate, respectively. In the SI and Wf models, the highest and lowest important parameters were the distance from river and geology. Flood susceptibility maps are informative for managers and decision makers in Haraz Watershed in order to contemplate measures to reduce human and financial losses.

K. Khosravi
Department of Watershed Management Engineering, Faculty of Natural Resources, Sari Agricultural Sciences and Natural Resources University, Sari, Mazandaran, Iran

H. R. Pourghasemi (✉)
Department of Natural Resources and Environmental Engineering, College of Agriculture, Shiraz University, Shiraz, Iran
e-mail: hamidreza.pourghasemi@yahoo.com

H. R. Pourghasemi
e-mail: hr.pourghasemi@shirazu.ac.ir

K. Chapi
Department of Watershed Management Engineering, Faculty of Natural Resources, University of Kurdistan, Sanandaj, Kurdistan, Iran

M. Bahri
Department of Watershed Management Engineering, Faculty of Natural Resources, Yazd University, Yazd, Iran

Keywords Flood susceptibility · Shannon's entropy · Statistical index · Weighting factor · GIS · Iran

Introduction

Generally, flash flood is defined as a rapid beginning of flood in a short time that mostly has a high peak

discharge; thus, this flood is usually caused by the rainfall that has a 1-h duration (Elkhrachy 2015). Annually, a variety of natural disasters such as floods, earthquakes, and landslides cause great damages to lives and properties throughout the world (Tierney et al. 2001; Tehrany et al. 2015a). The number of significant flood events in the world has meaningfully increased during the last three decades (Kourgialas and Karatzas 2011). Flood, which is the outcome of complex geological, geomorphological, and hydrological conditions, is probably the most devastating, widespread, and abundant natural disaster in the world (Gashaw and Legesse 2011) that leaves harsh socio-economic and environmental consequences behind (Wu and Sidle 1995; Glade 1998). The confluence of rivers is the prime place of concern for flood hazards (De Moel and Aerts 2011). As with the road flooding, the main concerns revolve around the damages mainly caused by high water levels after heavy rain showers in areas where rivers and roads intersect or where culverts and waterways are blocked by brushwood (Plate 2009). Intervention in natural conditions by human activities, such as road construction and timber harvesting, could increase the risk of occurrence of floods (Montgomery 1994; Chung et al. 1995). As a result of burgeoning population growth and the subsequent pressure, nature and behavior of floods have altered. Susceptibility to flood refers to the natural tendency to produce flood.

It should be noted that although flooding is inevitable and avoidance of it is impossible, the assessment and management of future floods can be achieved through proper analysis and forecasting methods (Cloke and Pappenberger 2009; Tehrany et al. 2015b). Identification of prone areas to floods or preparation of susceptibility maps of flooding is an important tool to mitigate future flood damages. Hence, by identifying locations with low susceptibility to flooding, suitable areas for developmental activities could be recognized (Sarhadi et al. 2012). Kourgialas and Karatzas (2011) state that flood management strategy consists of three phases: (1) pre-flood measures, (2) flood forecasting, and (3) post-flood activities; while Konadu and Fosu (2009) believe that the management of flood can be accomplished through four stages: anticipation, preparation, prevention, and damage assessment. Schanze (2006) divide flood risk management into flood risk assessment and mitigation. Obviously, strategies about impact of floods require identification of prone areas (Tehrany et al. 2013) to facilitate quick response,

decrease the impact of possible flood events, and provide a means for early warning (Kia et al. 2012).

Previous works

In recent years, several approaches have been developed by hydrologists to model flood risk and hazard (Jayakrishnan et al. 2005; Bahremand et al. 2007). In general, it should be noted that traditional hydrological methods have not been able to meet the needs of comprehensive flooding susceptibility assessment in regional studies (Li et al. 2012; Tehrany et al. 2015b); these methods are mainly based on linear assumptions that, in this case, are inappropriate for watershed studies with non-linear structures (Liu and De Smedt 2004; Tehrany et al. 2013). Application of RS and GIS has been a great evolution in environmental sciences such as landslides, groundwater resources, and flood susceptibility mapping and has also provided new insights into flood assessment studies. In general, several researchers have developed various techniques in the field of environmental studies by the application of GIS and RS.

Among different methods, the most popular and widely used models based on GIS in zoning different natural disasters include frequency ratio (Lee et al. 2012; Tehrany et al. 2013; Youssef et al. 2014), weights-of-evidence (Mohammady et al. 2012; Pourghasemi et al. 2012a), logistic regression (Pradhan 2010a; Akgun 2012; Felicísimo et al. 2012; Nampak et al. 2014), analytical hierarchy process (Chen et al. 2011; Althuwaynee et al. 2014; Kazakis et al. 2015), artificial neural network (Oh and Pradhan 2011; Kia et al. 2012), support vector machine (Tehrany et al. 2014b), decision trees (Tehrany et al. 2013), Shannon's entropy (Bednarik et al. 2010; Pourghasemi et al. 2012c; Sharma et al. 2013; Jaafari et al. 2014), weighted factor (Yalcin et al. 2011), statistical index (Pourghasemi et al. 2013), and fuzzy logic (Pourghasemi et al. 2012b).

Kazakis et al. (2015) in a study entitled the assessment of flood hazard areas at a regional scale in Greece used index-based approach and AHP models. Finally, a comparison between the flood maps was produced and the historical events showed that the model was capable of flood hazard mapping.

Tehrany et al. (2015a) combined the two support vector machine (SVM) and frequency ratio (FR) models in the Kelantan Watershed. The results showed that the hybrid model had slightly better performance than the DT model.

Tehrany et al. (2015b), using SVM models with four different functions, prepared the susceptibility maps of flooding in the Kuala Terengganu Watershed in Malaysia. They finally stated that SVM-RBF model with the AUC of 84.97% had the highest level of accuracy among four different functions. By measuring Cohen's kappa, the researchers claimed that, except for surface runoff factor, other factors had a positive impact on flooding.

Youssef et al. (2016) performed an analysis on the susceptibility to flooding in Jeddah, Saudi Arabia, by applying FR and LR methods and their combination. They stated that the hybrid approach, with the AUC of 91.3%, had been more reliable and accurate than the FR model with the AUC of 89.6%.

According to the literature mentioned above, the Shannon's entropy data-mining technique is one of the new methods applied in environmental sciences such as groundwater and landslide studies. Yet, this approach is new to the flooding assessment studies. Application of the statistical index (SI) and weighting factor (Wf) is completely novel in the field of flood susceptibility zoning, while it has been commonly used in the landslide hazard assessment. Hereby, the aim of this study is flood susceptibility mapping in the Haraz Watershed, Mazandaran Province, by deploying Shannon's entropy, statistical index, and weighted factor methods. The efficiency of these models will also be taken into account. One of the other objectives of this study is to determine which factors have the highest impact on the incidence of flooding in the study area. This watershed witnesses many floods annually that cause widespread losses and property damages. Despite the fact, no appropriate measures have been contemplated in these areas to prevent or mitigate the damages.

Study area

The Haraz Watershed is located in Amol County, between 51° 43' to 52° 36' E and 35° 45' to 36° 22' N. The total area enclosed in this watershed measures roughly 4015 km². The elevation ranges from 328 m at the bottom to about 5595 m at the rim. Nour, Akhensar, Shirkolaroud, and Namarestagh are some of the main rivers flowing in the area. Major elevations of the area include the mounts of Damavand, Shimkouh, Emamzadeh Ghasem, Yakhli, Zanjirband, and Lou. The main settlement areas are Polor, Nashal, Tiran, Rineh, Kandovan, Ab-e-Ask, Gazanak, Baijan,

Belghalm, Belde, and Nour. Figure 1 provides an overview of the study area. Due to extreme flood incidences and the resulting life and property damages, the Haraz Watershed has been chosen as the case study area.

Methodology

According to Tehrany et al. (2014b), the analysis of susceptibility to flooding is one of the most imperative issues in river hydrology, which has been carried out in the current study by considering three methods of SE, SI, and Wf in the Haraz Watershed. The flowchart of this research is presented in Fig. 2.

Data collection

Flash flood historical mapping

Flood inventory maps are necessary for the study of the relationship between floods and their causative factors. To prepare flood susceptibility map, the first step is to obtain the appropriate data and create a spatial database. It is vital to provide the necessary data with high accuracy (Jebur et al. 2013). In this study, flood inventory map was prepared by the historical floods of 2002, 2006, and 2013 according to the documentary sources and extensive field inventories. In the meantime, a total of 211 flood points on the scale of 1:25,000 were identified, as shown in Fig. 1.

Causative factors

To develop a methodology for evaluating the susceptibility to flooding, it is necessary to determine the causative factors and their relationship with flood occurrences (Liu and De Smedt 2005; Pradhan 2009). In fact, regional assessment of floods should be practical and applicable for the study area; thus, the input parameters should represent reliable and simply achievable factors (Oh and Pradhan 2011). For this study, ten flood causative factors were selected based on literature review, as follows: slope angle, plan curvature, altitude, topographic wetness index (TWI), stream power index (SPI), distance from river, rainfall, geology, land use, and normalized difference vegetation index (NDVI) (Figs. 3a–j). All factors were subsequently converted into raster maps with the pixel sizes (resolution) of 20 × 20 m.

Digital elevation model (DEM), as a principal source for extracting topographic factors, is one of the most

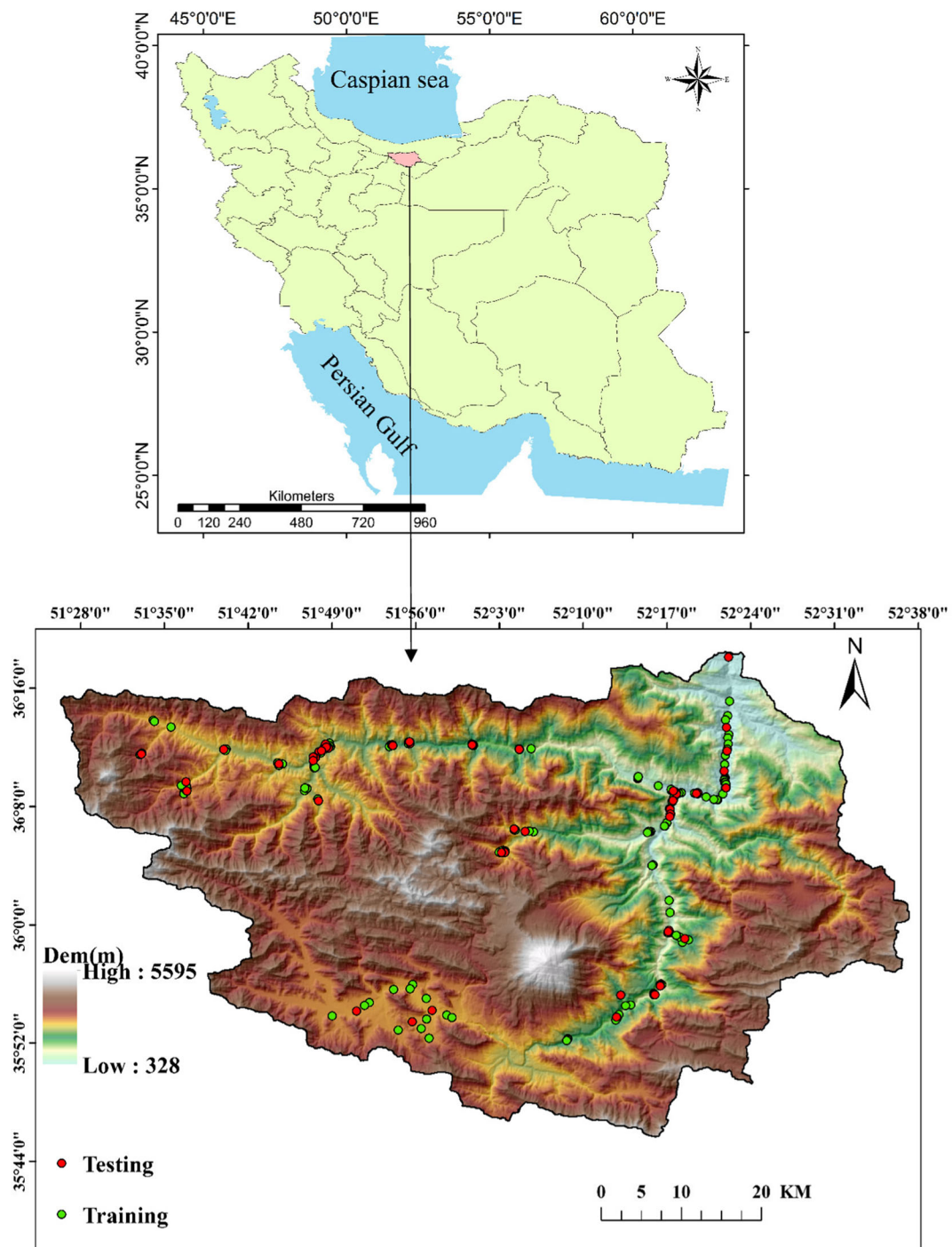
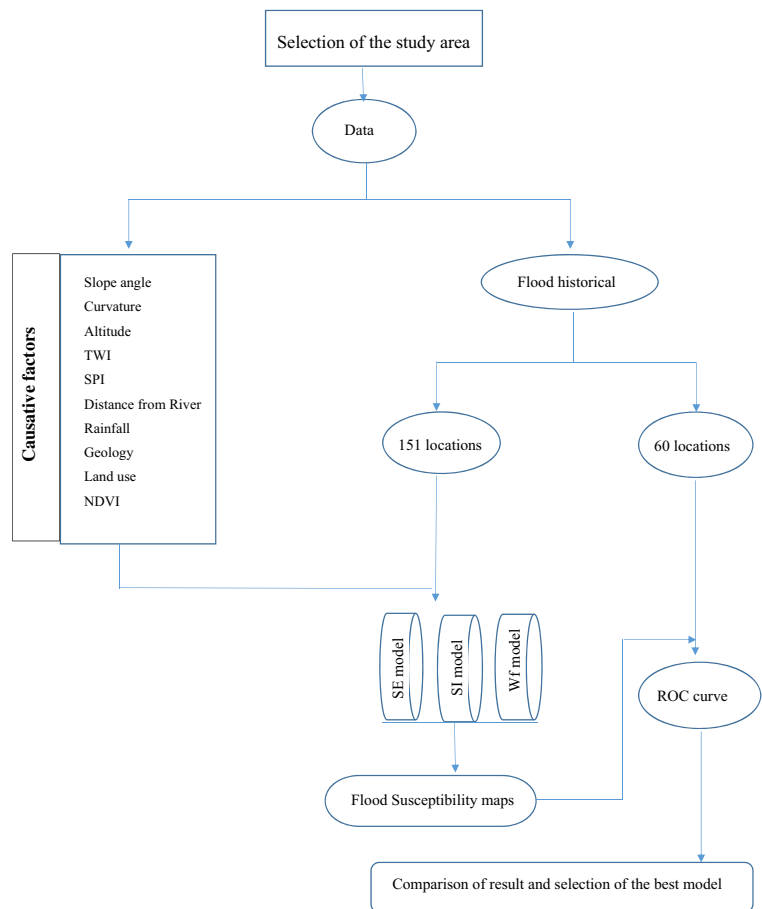


Fig. 1 Location of flooding point. Case study position and its hillside

important flood causative factors which has been used in various research works (Tehrany et al. 2013; Youssef et al. 2014). Topography plays an absolutely crucial role in spatial variability of hydrological conditions such as

soil moisture and groundwater flow. Extracted topographical factors include slope, plan curvature, altitude, TWI, and SPI. One of the most important factors affecting flood in the area is slope (Tehrany et al. 2013). As

Fig. 2. Flow chart of methodology in this research



slope steepness increases, the rate of water infiltration is reduced and the velocity of water increases; hence, huge volume of runoff reaches the river and flat area and leads to flooding. Thus, any increase in slope gradient could result in more runoff and increase in its velocity, but floods commonly take place in areas with less slopes. Slope map of the region was divided into five classes ranging from 0° to 66.8°, which are shown in Fig. 3a. Plan curvature is another important factor for flooding. In this regard, flat areas have become exposed to the highest potential of flood occurrence. The plan curvature represents the morphology of the topography; therefore, to map the plan curvature in GIS, negative values were treated as Concave, zero as flat and positive numbers as convex surfaces (Oh and lee 2010). As noted, the plan curvature map was divided into three classes, which are shown in Fig. 3b. Another important factor for flood occurrence is altitude. The research conducted by Botzen et al. (2013) states that the occurrence of flood is almost impossible in high altitudes. Altitude of

the area was accordingly classified into nine classes ranging from 328 to 5595 m, as illustrated in Fig. 3c. TWI represents the accumulation of flow at any point in the catchment area as the result of the runoff tendency to travel down the slope by the force of gravity (Gokceoglu et al. 2005), and this is closely related to the soil moisture content.

SPI represents the erosive power of water flow (Jebur et al. 2014). TWI and SPI maps were prepared in SAGA-GIS Software and finally divided into ten classes, which are shown in Fig. 3d, e. Another very important factor that is considered in this research is distance from the river (Fig. 3f), as it affects the velocity and extent of floods in the region (Glenn et al. 2012). Precipitation map was prepared from 20-year rainfall data records of 17 rain gauges (Khosravi et al. 2016) and then was classified into nine classes (Fig. 2g). Geological layers were acquired in the shape file format from the Regional Water Department of Sari City. This factor was reproduced from the geological map at a scale of 1:100,000. Geological map was classified

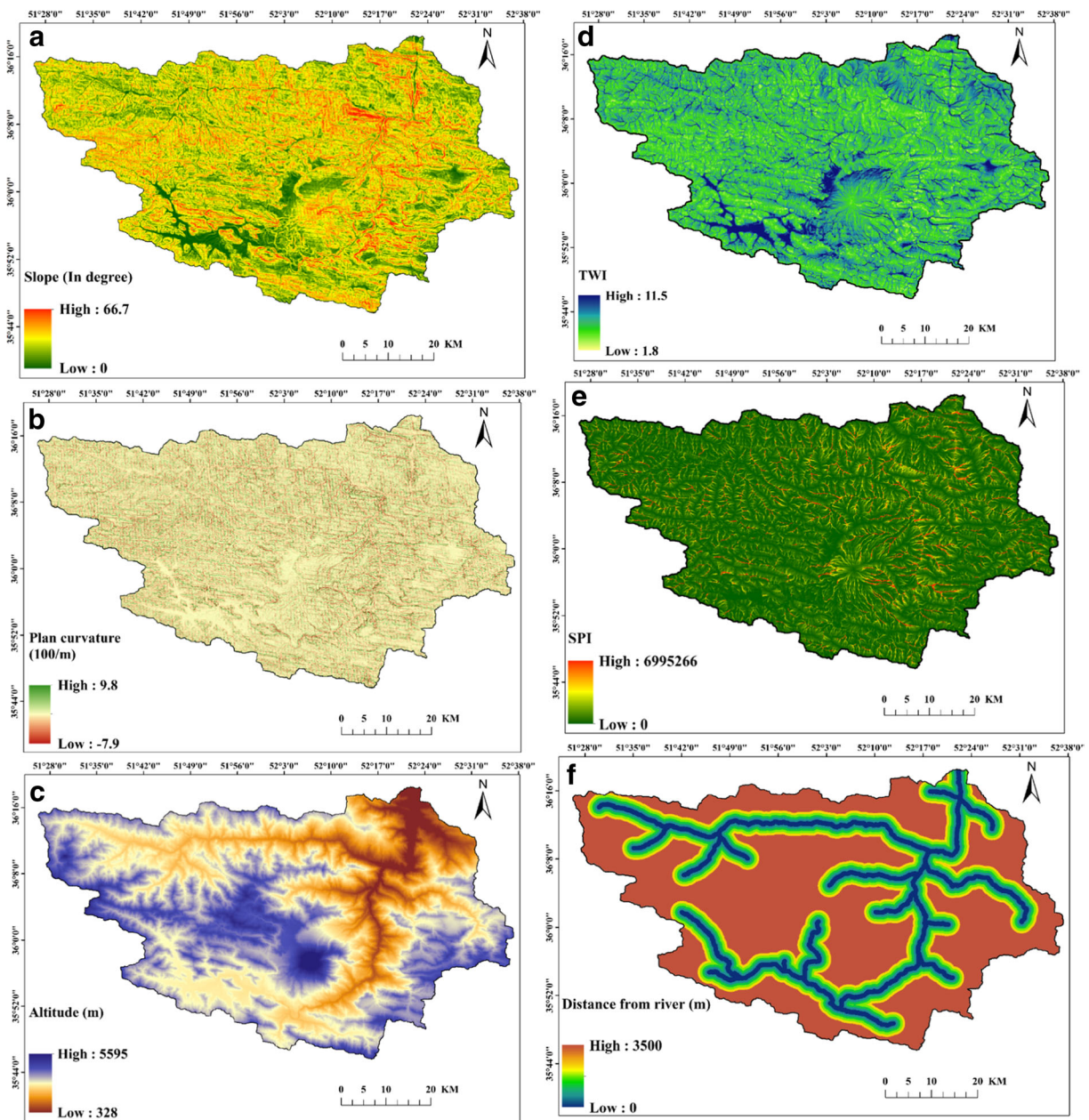


Fig. 3 Flood causative factors in Haraz Watershed: **a** slope angle, **b** plan curvature, **c** altitude, **d** topographic wetness index TWI, **e** stream power index SPI, **f** distance from river, **g** rainfall, **h** geology, **i** land use, and **j** NDVI

into three classes including Mesozoic, Paleozoic, and Cenozoic (Fig. 2h). Geological characteristics of the study area are summarized in Table 1. Most of the mountains and reliefs in the region, such as Damavand, are within the Cenozoic class. Using the Operational Land Imager (OLI) sensor images of the Landsat 8 satellite, land use and NDVI maps were prepared for year 2013 in ENVI 5.1 software. For land use mapping, neural network algorithms

and supervised classification were applied. Land use map was divided into seven classes of water bodies, residential, rangeland, orchards, irrigated land, forest, and bare land (Fig. 2i). The majority of the watershed was devoted to the rangeland class. The range of NDVI index values varied between +1 and -1 that show a measure of vegetation characteristic of an area. The negative values indicating the water, values close to zero (-0.1-0.1) show the barren

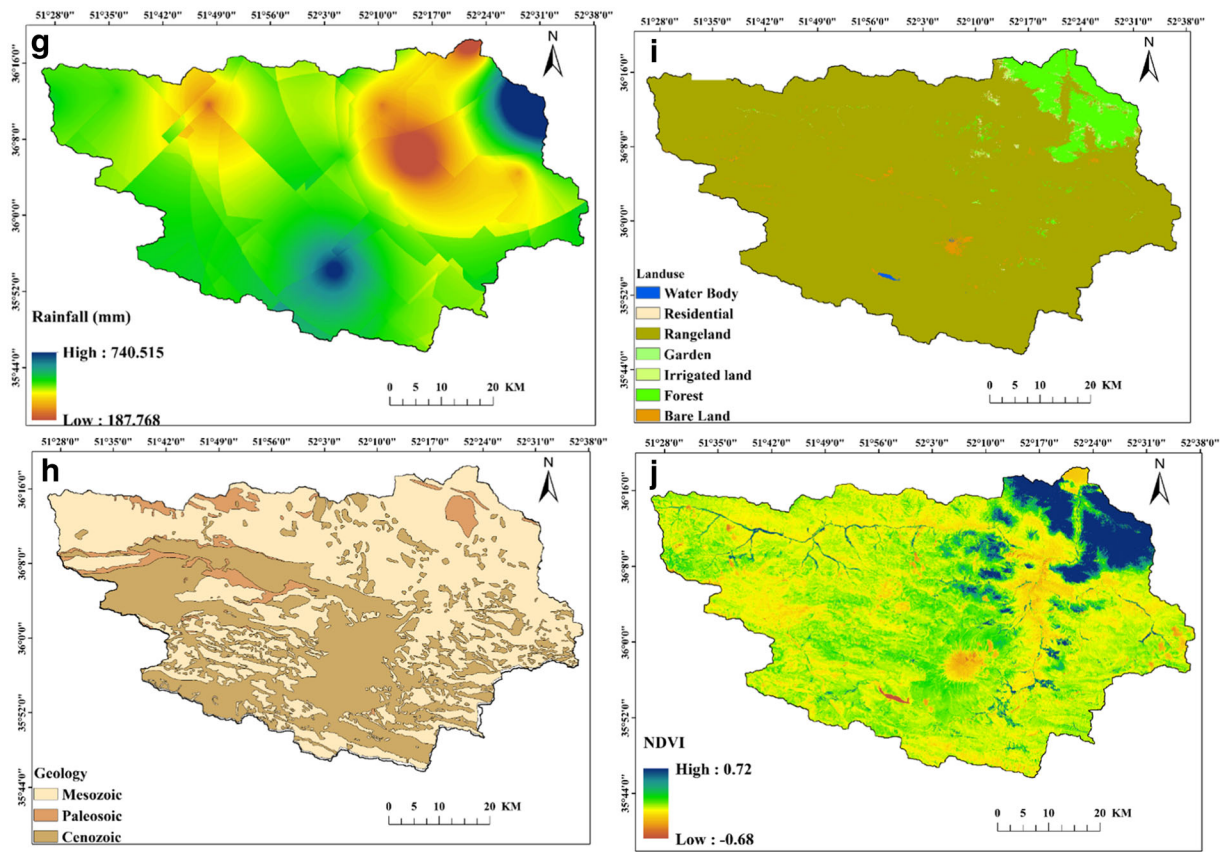


Fig. 3 (continued)

areas, low positive values (0.2–0.4) represent the grasslands and shrub, and high values show the rainforests and dense forest. NDVI index map was divided into ten classes (Fig. 2j).

Application of BSA

Shannon’s entropy model

Entropy is a measure of disorder, instability, imbalanced behavior, energy distribution, and uncertainty in a system (Yufeng and Fengxiang 2009; Pourghasemi et al. 2012a). In sum, entropy means the quantity of irregularities between causes and results or decisions on various debated topics (Wan 2009). Entropy is the representation of evenness, in which the groups are equally and uniformly distributed among organizational units (Massey and Nancy 1988). Entropy index is regarded as a measure of the average difference of the proportion of unit groups from the total system (Theil 1972;

Naghibi et al. 2014). Shannon entropy is function of probability distribution and the criterion for measurement of the amount of its uncertainty (Hosseinpoor Milaghardan and Abbaspoor 2015) as follows:

$$E_i = S(P_1, P_2, \dots, P_n) = -M \sum P_i \ln P_i \quad i = 1, 2, \dots, n \tag{1}$$

where P_i is probability distribution function and M is the constant value for adjustment of entropy (between 0 and 1) (Eq. 1). If all the values of P_i equal each other ($P_1 = P_2 = \dots = P_n$), then for all of the i and j values (Asgharzadeh and Nasrolahi 2006), calculation is as follows:

$$P_i = 1/n \tag{2}$$

If there are n alternatives and k criteria in the decision matrix, the result of the matrix for the j th criterion is calculated as follows:

Table 1 Lithology of the Haraz Watershed

Lithology	Code	Era	
Undifferentiated Quaternary deposits	Q	Cenozoic	
Loose alluvium in the river channels	Qal		
Rock fall	Qf		
Landslide	Qlan		
Moraines (glacial deposits)	Qm		
Scree, talus fans	Qs		
Scree	Qsc		
Marine conglomeratic terraces	Qt		
Old terraces	Qt1		
Younger gravel fans and terraces	Qt2		
Loess	Qt2c		
Sinter deposits	Qtr		
Basalt and olivine	Qv1		
Agglomerate and andesite tuff	Qv2		
Damavand magma, andesite trachyte	Qv3		
Quartz-diorite	Qd		
Rhyolite	Rh		
Trachyte	TR		
Dacite	da		
Marl, Mila formation	E-m		
Pyroclastic and andesite, Karaj formation	EA		
Conglomerate, Fajan formation	Ef		
Gypsum	Eg		
Tuff, volcanic rock	Ek		
Nummulitic limestone	Ez		
Dacite, pyroclastic with	Ezt2		
Calcareous and siliceous shales	Eksl		
Middle tuff member: pyroclastics	Ekt2		
Trachyandesite, trachybasalt, basanite	Evkt2		
Santonian limestone	K2 1		Mesozoic
Limestone, marl, limestone, silty marl	K2plm		
Cast locally with the layers of dolomitic limestone and shale	Kgl		
Limestone and marl	Kl-m		
Orbitolina limestone	Klt		
Basalt	Kv		
Basalt, diabase, pyroclastic rocks	Kv1		
And pyroclastic volcanic rocks are not separated	Kv1 ,2		
Tuff, basaltic andesite pyroclastic	Kv2		
Cut from multiple sources, Paland formation	TRb		
A thin layer of cream limestone, shale, limestone, Elika	TRe1	Paleozoic	
Thick dolomite to form massive, limestone	TRe2		
Mafic volcanic rocks	TRv3		
Gabbro	Tgb		
Rocks, marl, conglomerate, Paleocene	Peef		
Sandstone, shale, limestone, quartzite, make peace	Pefvmc		
Rocks, marl, conglomerate, Paleocene	Pd		
Limestone, marly and sandy shales	Pn		
Fusulina limestone, dolomitic limestone	Pr		
Basic flow, pyroclastics	Pv		

$$P_{ij} = \frac{f_j(ai)}{\sum_{i=1}^n f_j(ai)}; \quad j = 1, 2, \dots, n \quad \forall j \quad (3)$$

There is a one-to-one relationship between the quantity and value of the system entropy and the level of irregularity that is called Boltzmann principle and is commonly used to display the thermodynamic condition of a system (Yufeng and Fengxiang 2009). Shannon has been modified based on the Boltzmann model, and it uses the entropy model for the theory of information (Pourghasemi et al. 2012a). Several important factors introduce excess entropy to the system. Entropy values can be used to calculate the target weight of the index system (Yang et al. 2010). Shannon entropy (SE or E_j) can be calculated as:

$$E_i = -M \sum_{i=1}^n P_{ij} \ln P_{ij}; \quad \forall j \quad (4)$$

$$M = \frac{1}{\ln n} \quad (5)$$

where n is the number of that; in this study, it is the number of classes for each causative factor. Degree of diversification (d_j) shows how much proper information the j th criterion gives to the decision maker.

$$d_j = 1 - E_j; \quad \forall j \quad (6)$$

Finally, the weight could be calculated based on Eq. 7 as follows:

$$V_j = \frac{d_j}{\sum_{j=1}^n d_j}; \quad \forall j \quad (7)$$

Statistical index model

The SI bivariate statistical method has been introduced by van Western (1997) for landslide susceptibility mapping. It requires selection and mapping of the important parameters and their classification into relevant classes, flood inventory mapping, overlaying the flood inventory map with each causative factor, determination of the density of floods in each class of parameters, and calculation of weight values. Subsequent steps are assigning the values to various parameters, overlaying layers, and

preparation of the final susceptibility map for each land unit (Aleotti and Chowdhury 1999; Yalcin 2008). Weight values for each class of parameters are calculated as the natural logarithm of flood density of the class divided by the total flood density of the map (Van Westen 1997; Rautela and Lakhera 2000; Cevik and Topal 2003; Pourghasem et al. 2013). Implementation of SI method is based on the following equation (Van Westen 1997):

$$W_{SI} = \text{Ln}\left(\frac{E_{ij}}{E}\right) = \text{Ln}\left(\frac{L_{ij}/L_T}{P_{ij}/P_L}\right) \tag{8}$$

where W_{SI} is the assigned weight to the given class i of the parameter j ; E_{ij} is the flood density in the class i of the parameter j ; E denotes the total flood density within the entire map; L_{ij} is the number of flooding locations in the class i of the parameter j ; L_T is total number of floods in the entire map; P_{ij} is the number of pixels in the class i of the parameter j ; and P_L is the total number of pixels in the entire map.

This method is based on statistical correlation between the flood inventory map and characteristics of various parameters (Yalcin 2008). In this study, all of the parameters were crossed with the flood inventory map, and the resulting flood density in each class of parameters of interest was calculated. The correlation outcomes were sorted in the resultant raster, and flood density was calculated for the classes of parameters. The SI values were calculated for each of the features. Finally, flood susceptibility mapping was performed by overlaying the different layers.

Positive values of W_{SI} indicate the proper and robust relationship between the classes and flooding distribution such that the stronger the relationship is, the higher the score will become. Negative values for W_{SI} mean that there is no correlation between the class and the flood occurrence.

Weighting factor model

As the FR model for determination of its weights used the SE model, Wf model utilizes the SI value to determination of its weights. In other words, Wf method can be regarded as the modified version of the statistical index (Cevik and Topal 2003; Oztekin and Topal 2005; Yalcin 2008). In these methods, the Wf weights are calculated by the procedures that SI considers for

determination of each attribute and each SI weight. Firstly, flood inventory map is rasterized, and then, it is crossed with other rasterized parameters. SI values are calculated for each flood pixel in each layer. Then, the values of all the pixels belonging to each layer are summed. Eventually, the weighting factor values for each layer are calculated in a range of 1 to 100 by the following equations (Yalcin 2008; Yalcin et al. 2011).

$$TSI = \sum_{i=1}^n SI \times S_{.pix} \tag{9}$$

$$W_{Wf} = \frac{(TSI_{value}) - (MinTSI_{value})}{(MaxTSI_{value}) - (MinTSI_{value})} \times 100 \tag{10}$$

where TSI is the total value of the flooding pixels of a given class of parameters of interest, n the number of classes of the parameter, W_{Wf} the weight factor for each layer of maps (final weight), MinTSI the minimum value of the total weights among the layers, and MaxTSI maximum value of the total weights among the layers. Wf values of each layer are multiplied by SI values of the classes of the maps. At last, all the factors are added together and flood susceptibility map is prepared according to the Wf method (Yalcin 2008; Yalcin et al. 2011).

Result and discussion

FSM using SE model

Shannon’s entropy results with the relationship between the occurrence of floods and the flood factors are shown in Table 2. Slope angle, plan curvature, and altitude were given weights equal to 0.719, 0.134, and 1.711, respectively, which reflect the fact that among topographical factors, the most important factor is altitude followed by slope angle and plan curvature.

TWI and SPI were assigned weights of 0.388 and 1.054, indicating that the SPI was the most important factor among the hydrological factors. The calculated weights for other causative factors were as follows: distance from river (1.236), rainfall (0.365), geological condition (0.008), land use (1.09), and NDVI (1.89). Overall, the most and the least important factors for flooding were distance from river and geology, respectively. Finally, the flood susceptibility mapping (FSM)

prepared by SE (Fig. 4a; Eq. 11) showed that very low, low, medium, high, and very high covered 13.57, 26.66, 30.04, 21.53, and 8.17% of the area, respectively.

$$\begin{aligned}
 \text{FSM}_{\text{SE}} = & 0.719 \times \text{slopeangle} + 0.134 \\
 & \times \text{plancurvature} + 1.711 \times \text{altitude} + 0.388 \\
 & \times \text{TWI} + 1.084 \times \text{SPI} + 2.11 \\
 & \times \text{distancefromriver} + 0.554 \times \text{rainfall} + 0.008 \\
 & \times \text{geology} + 1.091 \times \text{landuse} + 1.899 \\
 & \times \text{NDVI} \quad (11)
 \end{aligned}$$

FSM using SI model

Weights derived by this procedure for each class of each layer are shown in Table 3. According to Table 3, for slope angle classes of 0–5.7 and 5.7–15.9, positive weight values of 1.78 and 0.78 have been obtained, respectively, while higher slope classes have gained negative weights, indicating that higher correlation values between the occurrence of floods and the class would result in larger positive values and lower correlation values between the occurrence of floods and the class would result in low and negative values.

Naturally, because the flood occurs in an area with low slope, the weights that are obtained using SI method should be positive for low slope with decrease in slope and the SI value should increase. The value for the convex class of the plan curvature parameters was negative, while it was positive for the other two classes (concave = 0.51 and flat = 0.14). With respect to these weights, it can be concluded that the concavely curved and flat surfaces are more likely prone to flooding than the convex surfaces, which corresponds to the findings of Tehrany et al. (2015a, b). In case of altitude, 328–2456 and 2456–2770 m obtained positive and negative weights, respectively, while no flood occurrence was recorded for higher altitudes. The highest weight was for the low-altitude class (1141–328 m), which is consistent with the normal behavior of flood in reality. For lower values of TWI Factor, negative weights were obtained; while for higher values, positive weights were obtained. In general, we can say that by increasing TWI, the probability of flooding increases. The highest weight obtained was equal to 1.69, corresponding to the TWI of

7.1–8. The flooding locations recorded for model training for the SPI factor occurred in the range of 0 to 1,810,539 with no registered floods for higher values. In the domain of flooding locations, by increasing the SPI value, high weight was acquired. For lower SPI values in the range of 0 to 27,432, negative weight was obtained, while the maximum weight occurred in the range of 1,234,458 to 1,810,539.

The sixth factor considered in this study was distance from river, which according to the review of literature, was one of the most important factors affecting floods (Tehrany et al. 2015b). For this parameter, only the first class (i.e., 0 to 500 m) gained positive weight, while other classes were negatively weighted; this reduction of weight was held by succeeding farther from the river. Thus, by this interpretation, with increasing distance from the river, the probability of flooding decreases.

For the rainfall factor, increase in rainfall resulted in smaller weights, meaning reduced probability of flooding by increasing rainfall. This is best explained by the fact that higher altitude receives higher precipitation, while these areas are marked with much less probability of flooding. Positive weights were obtained for three classes of 183–267, 267–329, and 329–375 mm, turning into negative values for the next three classes from 375 to 468 m with no registered flooding for precipitation exceeding 468 mm.

Haraz Watershed geology consists of Paleozoic, Mesozoic, and Cenozoic formations weighted 0.23, 0.02, and –0.06, respectively. By this notion, the geology formations of Paleozoic are the primary factor affecting flooding due to higher positive weight, with Cenozoic unit as the least important. For land use, the maximum weights were of the water bodies at 3.57, followed by bare lands at 2.1, and finally residential areas at 1.04. For rangeland with a weight of –0.06 and forest with –0.58, there is negative correlation between these factors and floods. Despite the presence of 132 out of 151 flood locations in the rangeland areas, the weight value was negative due to extensive rangeland cores compared with the distribution of flooding locations. In orchards and agricultural land use types, no flood situations have been registered. The last intended factor was NDVI, which for Haraz Watershed obtained a range of –0.69 and –0.58. No special relationship cannot be established between these parameters and the positive and

Table 2 Spatial relationship between flood causative factors and flooding locations using SE

Class	No. pixels in domain	Percentage of domain	No. of floods	Percentage of floods	FR	E_{ij}	H_j	H_{jmax}	I_j	V_j
Slope angle										
0–5.7	527,064	5.31	47	31.12	5.86	0.662	1.379	2.322	0.406	0.719
5.7–15.9	2,278,837	22.95	70	46.35	2.02	0.228				
15.9–24.6	3,019,849	30.41	22	14.57	0.48	0.054				
24.6–33.25	2,788,907	28.09	4	2.64	0.09	0.011				
33.25–66.77	1,315,332	13.25	8	5.29	0.40	0.045				
Plan curvature (100/m)										
Convex	4,045,570	40.74	23	15.23	0.37	0.118	1.384	1.585	0.127	0.134
Flat	2,545,930	25.64	44	29.13	1.14	0.359				
Concave	3,338,493	33.62	84	55.62	1.65	0.523				
Altitude (m)										
328–1141	337,377	3.40	59	39.073	11.50	0.654	0.394	3.170	0.876	1.711
1141–1658	653,985	6.59	18	11.921	1.81	0.103				
1658–2093	841,869	8.48	31	20.530	2.42	0.138				
2093–2456	1,259,033	12.68	22	14.570	1.15	0.065				
2456–2770	1,976,235	19.90	21	13.907	0.70	0.040				
2770–3075	1,998,538	20.13	0	0.000	0.00	0.000				
3075–3417	1,696,868	17.09	0	0.000	0.00	0.000				
3417–3954	1,048,316	10.56	0	0.000	0.00	0.000				
G > 3954	117,797	1.19	0	0.000	0.00	0.000				
TWI										
1.8–3.7	1,064,318	10.72	3	1.987	0.19	0.009	2.713	3.322	0.183	0.388
3.8–4.1	2,232,092	22.48	3	1.987	0.09	0.004				
4.2–4.5	2,037,114	20.51	8	5.298	0.26	0.012				
4.6–4.9	1,835,184	18.48	18	11.921	0.65	0.031				
5–5.3	1,216,401	12.25	33	21.854	1.78	0.084				
5.4–5.7	770,366	7.76	32	21.192	2.73	0.129				
5.8–6.2	493,239	4.97	40	26.490	5.33	0.252				
6.3–7	185,713	1.87	8	5.298	2.83	0.134				
7.1–8	61,325	0.62	5	3.311	5.36	0.254				
8.1–11.5	34,257	0.34	1	0.662	1.92	0.091				
SPI										
0–27,432.4	8,389,309	84.97	84	55.629	0.65	0.022	2.100	3.322	0.368	1.084
27,432.4–164,594.4	1,039,060	10.52	32	21.192	2.01	0.068				
164,594.4–411,486.2	260,354	2.64	21	13.907	5.27	0.179				
411,486.2–768,107.5	106,583	1.08	8	5.298	4.91	0.167				
768,107.5–1,234,458.6	45,996	0.47	2	1.325	2.84	0.096				
1,234,458.6–1,810,539.3	18,981	0.19	4	2.649	13.78	0.468				
1,810,539.3–2,496,349.6	7739	0.08	0	0.000	0.00	0.000				
2,496,349.6–3,319,322	3518	0.04	0	0.000	0.00	0.000				
3,319,322–4,745,807.5	1791	0.02	0	0.000	0.00	0.000				
4,745,807.5–6,995,265.5	272	0.00	0	0.000	0.00	0.000				

Table 2 (continued)

Class	No. pixels in domain	Percentage of domain	No. of floods	Percentage of floods	FR	E_{ij}	H_j	H_{jmax}	I_j	V_j
Distance from river (m)										
0–500	945,165	9.52	128	84.76	8.91	0.868	0.809	2.585	1.236	2.115
500–1000	889,321	8.96	9	5.96	0.67	0.065				
1000–1500	858,482	8.64	5	3.31	0.38	0.037				
1500–2000	827,818	8.34	2	1.32	0.16	0.015				
2000–2500	798,718	8.04	1	0.66	0.08	0.008				
>2500	5,611,062	56.50	6	3.97	0.07	0.007				
Rainfall (mm)										
183–267	49,519	0.50	4	2.65	5.31	0.403	2.014	3.170	0.365	0.534
267–329	366,418	3.69	26	17.22	4.67	0.354				
329–375	1,876,230	18.90	35	23.18	1.23	0.093				
375–409	4,310,056	43.41	62	41.06	0.95	0.072				
409–434	2,252,289	22.69	19	12.58	0.55	0.042				
434–468	701,730	7.07	5	3.31	0.47	0.036				
468–514	231,312	2.33	0	0.00	0.00	0.000				
514–576	78,768	0.79	0	0.00	0.00	0.000				
>576	61,831	0.62	0	0.00	0.00	0.000				
Geology										
Cenozoic	3,857,722	38.84	55	36.42	0.94	0.291	1.573	1.585	0.007	0.008
Mesozoic	5,604,514	56.43	87	57.62	1.02	0.317				
Paleozoic	469,735	4.73	9	5.96	1.26	0.391				
Land use										
Rangeland	9,189,569	92.54	132	87.42	0.94	0.020	1.181	1.404	0.159	1.091
Bare land	72,487	0.73	9	5.96	8.17	0.170				
Forest	592,322	5.96	5	3.31	0.56	0.012				
Garden	13,007	0.13	0	0.00	0.00	0.000				
Residential	23,406	0.24	1	0.66	2.81	0.058				
Irrigation	32,539	0.33	0	0.00	0.00	0.000				
Water body	7391	0.07	4	2.65	35.59	0.740				
NDVI										
–0.69 to –0.35	11,325	0.11	5	3.31	29.01	0.616	1.983	3.322	0.403	1.899
–0.34 to –0.18	245,042	2.47	7	4.64	1.88	0.040				
–0.17 to –0.13	1,503,258	15.15	17	11.26	0.74	0.016				
–0.12 to –0.08	3,142,579	31.67	15	9.93	0.31	0.007				
–0.07 to –0.03	2,806,738	28.29	32	21.19	0.75	0.016				
–0.02 to 0.05	1,061,917	10.70	22	14.57	1.36	0.029				
0.06 to 0.18	332,396	3.35	15	9.93	2.97	0.063				
0.19 to 0.33	239,320	2.41	20	13.25	5.49	0.117				
0.34 to 0.47	251,095	2.53	16	10.60	4.19	0.089				
0.48 to 0.73	328,562	3.31	2	1.32	0.40	0.008				

Note: FR is the frequency ratio; E_{ij} is the probability density; H_j and H_{jmax} are the entropy values; I_j is the information value; and V_j depicts the resultant weight value for the parameter as a whole

negative weights. In the ten classes related to this factor, the weight for the first two classes was positive; for the next three classes was negative;

for the next four classes was positive; and for the final class was negative. The highest weight was for the first class with a range of –0.35 to –0.69

and with the weighting of 3.38. Finally, according to Eq. 12, map of flood susceptibility by the SI method (Fig. 4b) was created:

$$\begin{aligned}
 \text{FSM}_{\text{SI}} = & \text{slope angle}_{\text{SI}} + \text{plan curvature}_{\text{SI}} \\
 & + \text{altitude}_{\text{SI}} + \text{TWI}_{\text{SI}} + \text{SPI}_{\text{SI}} \\
 & + \text{distance from river}_{\text{SI}} + \text{rainfall}_{\text{SI}} \\
 & + \text{geology}_{\text{SI}} + \text{landuse}_{\text{SI}} + \text{NDVI}_{\text{SI}} \quad (12)
 \end{aligned}$$

The map was classified based on the natural break classification scheme into low, low, moderate, high, and very high susceptibility classes.

Most of the area, by 31.17%, was devoted to the low susceptibility to flooding, while the least area was identified by the very high susceptibility of 0.58% (22.07 km²). The area with high susceptibility to flooding covered 662.2 km² that equals 17.57% of the study area.

FSM using Wf model

The last method considered for assessment of susceptibility to flooding in the Haraz Watershed was the Wf approach. The weights obtained by this approach can be attained from the SI method; put simply, WF method receives its weights from the SI method and the final weight is calculated as the combination of the both weights shown in Table 3. The Wf method, same as SE method, is applicable for the calculation of the weights of the layers; but Wf method ranges from 0 to 100. In this method, the most important factors for the flooding were distance to river with a weight of 100, altitude with a weight of 71.4, TWI with a weight of 42.2, and slope angle with a weight of 40.1. The least important factor in the flooding, according to the results of the recent method, was geology. The map obtained from Eq. 13 was classified into five classes of susceptibility to flooding (Fig. 4c). Percent areas of the susceptibility classes of very low, low, moderate, high, and very high were 33.89, 28.25, 22.43, 9.3, and 6.1%, respectively.

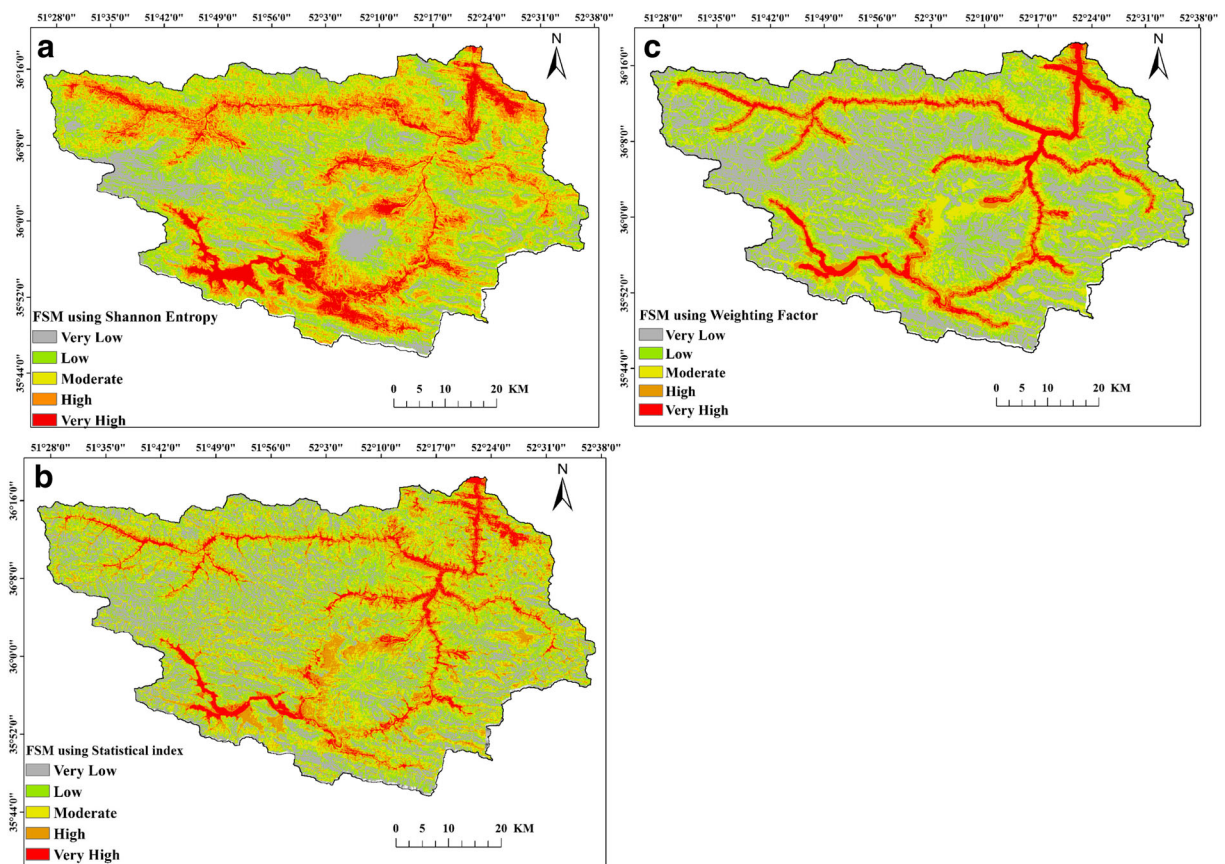


Fig. 4 Flood susceptibility mapping using **a** SE model, **b** SI model, and **c** WF model. F equal to flood and N equal to non-flood location

Table 3 Spatial relationship between flood causative factors and flooding locations using SI and Wf

Class	No. pixels in domain	Percentage of domain	No. of floods	Percentage of floods	SI	TWI	WF
Slope angle							
0–5.7	527,064	5.31	47	31.12	1.78	83.63	40.16
5.7–15.9	2,278,837	22.95	70	46.35	0.71	49.95	
15.9–24.6	3,019,849	30.41	22	14.57	–0.73	–15.96	
24.6–33.25	2,788,907	28.09	4	2.64	–2.35	–9.40	
33.25–66.77	1,315,332	13.25	8	5.29	–0.91	–7.25	
Plan curvature (100/m)							
Convex	4,045,570	40.74	23	15.23	–0.97	–22.39	10.59
Flat	2,545,930	25.64	44	29.13	0.14	6.09	
Concave	3,338,493	33.62	84	55.62	0.51	43.18	
Altitude (m)							
328–1141	337,377	3.40	59	39.073	2.45	144.72	71.42
1141–1658	653,985	6.59	18	11.921	0.60	10.87	
1658–2093	841,869	8.48	31	20.530	0.89	27.74	
2093–2456	1,259,033	12.68	22	14.570	0.15	3.29	
2456–2770	1,976,235	19.90	21	13.907	–0.35	–7.31	
2770–3075	1,998,538	20.13	0	0.000	None	None	
3075–3417	1,696,868	17.09	0	0.000	None	None	
3417–3954	1,048,316	10.56	0	0.000	None	None	
G > 3954	117,797	1.19	0	0.000	None	None	
TWI							
1.8–3.7	1,064,318	10.72	3	1.987	–1.67	–5.02	42.21
3.8–4.1	2,232,092	22.48	3	1.987	–2.42	–7.25	
4.2–4.5	2,037,114	20.51	8	5.298	–1.34	–10.75	
4.6–4.9	1,835,184	18.48	18	11.921	–0.43	–7.70	
5–5.3	1,216,401	12.25	33	21.854	0.59	19.45	
5.4–5.7	770,366	7.76	32	21.192	1.02	32.49	
5.8–6.2	493,239	4.97	40	26.490	1.68	67.38	
6.3–7	185,713	1.87	8	5.298	1.05	8.41	
7.1–8	61,325	0.62	5	3.311	1.69	8.45	
8.1–11.5	34,257	0.34	1	0.662	0.66	0.66	
SPI							
0–27,432.4	8,389,309	84.97	84	55.629	–0.41	–34.70	19.27
27,432.4–164,594.4	1,039,060	10.52	32	21.192	0.71	22.74	
164,594.4–411,486.2	260,354	2.64	21	13.907	1.67	35.14	
411,486.2–768,107.5	106,583	1.08	8	5.298	1.60	12.81	
768,107.5–1,234,458.6	45,996	0.47	2	1.325	1.06	2.11	
1,234,458.6–1,810,539.3	18,981	0.19	4	2.649	2.63	10.53	
1,810,539.3–2,496,349.6	7739	0.08	0	0.000	None	None	
2,496,349.6–3,319,322	3518	0.04	0	0.000	None	None	
3,319,322–4,745,807.5	1791	0.02	0	0.000	None	None	
4,745,807.5–6,995,265.5	272	0.00	0	0.000	None	None	
Distance from river (m)							
0–500	945,165	9.52	128	84.76	2.20	281.25	100
500–1000	889,321	8.96	9	5.96	–0.40	–3.57	
1000–1500	858,482	8.64	5	3.31	–0.95	–4.75	
1500–2000	827,818	8.34	2	1.32	–1.83	–3.66	
2000–2500	798,718	8.04	1	0.66	–2.49	–2.49	
>2500	5,611,062	56.50	6	3.97	–2.64	–15.87	
Rainfall (mm)							
183–267	49,519	0.50	4	2.65	1.68	6.72	14.63
267–329	366,418	3.69	26	17.22	1.55	40.32	

Table 3 (continued)

Class	No. pixels in domain	Percentage of domain	No. of floods	Percentage of floods	SI	TWI	WF
329–375	1,876,230	18.90	35	23.18	0.21	7.52	
375–409	4,310,056	43.41	62	41.06	−0.05	−2.80	
409–434	2,252,289	22.69	19	12.58	−0.58	−11.00	
434–468	701,730	7.07	5	3.31	−0.75	−3.74	
468–514	231,312	2.33	0	0.00	None	None	
514–576	78,768	0.79	0	0.00	None	None	
>576	61,831	0.62	0	0.00	None	None	
Geology							
Cenozoic	3,857,722	38.84	55	36.42	−3.53	−3.53	1
Mesozoic	5,604,514	56.43	87	57.62	1.81	1.81	
Paleozoic	469,735	4.73	9	5.96	2.08	2.08	
Land use							
Rangeland	9,189,569	92.54	132	87.42	−0.06	−7.57	9.33
Bare land	72,487	0.73	9	5.96	2.10	18.88	
Forest	592,322	5.96	5	3.31	−0.58	−2.91	
Garden	13,007	0.13	0	0.00	None	None	
Residential	23,406	0.24	1	0.66	1.04	1.04	
Irrigation	32,539	0.33	0	0.00	None	None	
Water body	7391	0.07	4	2.65	3.57	14.30	
NDVI							
−0.69 to −0.35	11,325	0.11	5	3.31	16.90	16.90	27.67
−0.34 to −0.18	245,042	2.47	7	4.64	4.50	4.50	
−0.17 to −0.13	1,503,258	15.15	17	11.26	−4.84	−4.84	
−0.12 to −0.08	3,142,579	31.67	15	9.93	−17.21	−17.21	
−0.07 to −0.03	2,806,738	28.29	32	21.19	−8.84	−8.84	
−0.02 to 0.05	1,061,917	10.70	22	14.57	7.06	7.06	
0.06 to 0.18	332,396	3.35	15	9.93	16.49	16.49	
0.19 to 0.33	239,320	2.41	20	13.25	34.31	34.31	
0.34 to 0.47	251,095	2.53	16	10.60	23.11	23.11	
0.48 to 0.73	328,562	3.31	2	1.32	−1.81	−1.81	

$$\begin{aligned}
 \text{FSM}_{\text{Wf}} = & 40.15 \times \text{slope angle}_{\text{SI}} + 10.58 \\
 & \times \text{plan curvature}_{\text{SI}} + 71.42 \times \text{altitude}_{\text{SI}} + 42.21 \\
 & \times \text{TWI}_{\text{SI}} + 19.26 \times \text{SPI}_{\text{SI}} + 100 \\
 & \times \text{distance from river}_{\text{SI}} + 14.63 \times \text{rainfall}_{\text{SI}} + 1 \\
 & \times \text{geology}_{\text{SI}} + 9.33 \times \text{landuse}_{\text{SI}} + 27.66 \\
 & \times \text{NDVI}_{\text{SI}} \tag{13}
 \end{aligned}$$

Validation of the FSMs

Validation is one of the primary and important steps in the development and evaluation of the obtained maps from different methods (Pourghasemi et al. 2012a), without which no models would be regarded as

scientifically sound (Chang and Fabbri 2003; Nampak et al. 2014). Efficiency of flood susceptibility model is usually estimated by independent information that is not available to build a model. The total of 211 flood locations recorded in the Haraz Watershed were randomly divided into two groups, 70% (151 location) and 30% (60 location), which were respectively used for the purposes of modeling and validation. In the current study, the following two methods were used for validation of the produced maps of susceptibility to flooding by the SE, SI, and Wf methods.

Histograms

To implement this method, in addition to the recorded floods, non-flooded locations were also utilized. For recording of 211 non-flooded locations as random spots on

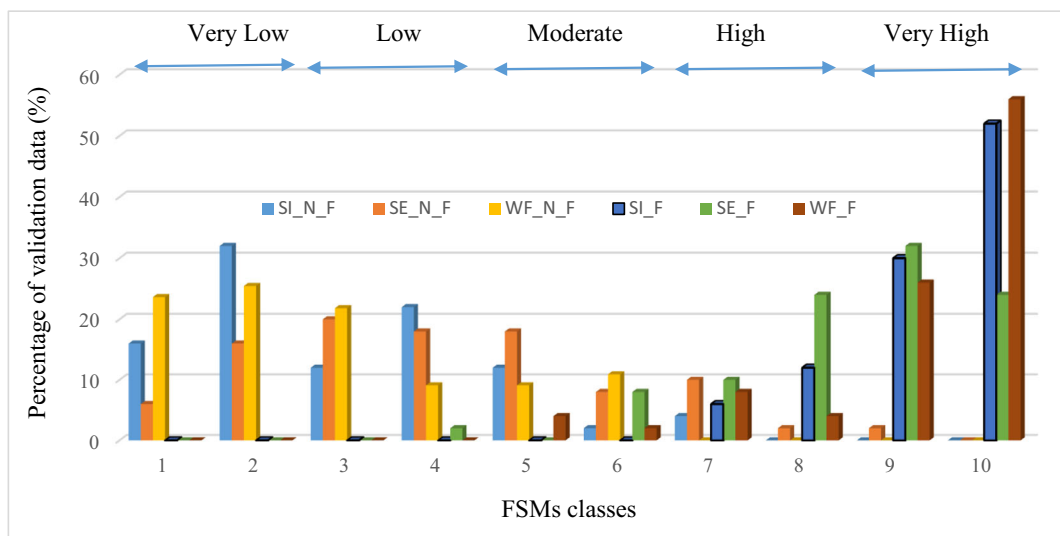
the hills, mountains, and places, where there were no flood events, Google Earth images were used (Tehrany et al. 2014a). Non-flooded locations were divided into two classes of 70% (151 positions) and 30% (60 locations); 30% of flooded and non-flood locations were used for the preparation of the histogram. Initially, susceptibility map was broken into ten levels (Dai and Lee 2002; Shirzadi et al. 2012); then, it overlaid the map of flooded and non-flooded locations and the final histogram was produced (as illustrated in Fig. 5). If the achieved maps are accurate, 30% of flood locations should be located in high-susceptibility classes (right wing of the graph) and 30% of non-flooded location should be located in low-susceptibility classes (left wing of the graph) (Meng et al. 2015). Therefore, no flooding locations must fall into the low to very low classes, and this also holds for the highly accurate and valid non-flooded locations. Thirty percent of the non-flooded locations must fall into the lower tails of the graph and must not fall into the high to very high classes; otherwise, the results of the model would not be sufficiently robust.

The results indicated that the Wf and SI models were comparatively more accurate, since most of the flooding locations fell into the high to very high susceptibility classes. However, given the other two classes, it is clear that the SI model is particularly accurate (there were flooding locations in the moderate class in the Wf method, while none was observed in the SI). SE model did not work properly (in comparison to SI and Wf) as there

were flooding locations, even in the fourth class, contributing to the low and very low susceptibility classes.

ROC curve

This method is one of the most popular (Pradhan 2010a, b; Pourghasemi et al. 2013; Tehrany et al. 2015a, b; Youssef et al. 2016) techniques to evaluate efficiency of the models, since it estimates the result of the model and quantitatively calculates efficiency. Prediction rate and success rates should be assessed as a necessary part of any program (Pourghasemi et al. 2012b). Thus, to evaluate the effectiveness and validity of FSMs, both success rate and prediction rate curves were produced using 70 and 30% of flooding locations, respectively (Youssef et al. 2016). Training data sets of floods were used in the production of flood maps; thus, success rate could not be used to assess the ability of the model (Pourghasemi et al. 2012b; Tehrany et al. 2015b; Youssef et al. 2016). Prediction rate, which is now widely used to measure and evaluate the performance and ability of the models (Lee et al. 2007; Tien Bui et al. 2011), was applied to efficiency of FSMs. Prediction rate indicates how well the model can predict floods in a given area. In this regard, 30% of non-flood locations that have been generated in the histogram section have been used there also. AUC of prediction rate can quantitatively measure the accuracy of model's prediction (Pradhan and Lee 2010). Figure 6a, b denotes success rate and prediction



- F equal to flood and N equal to non-flood location

Fig. 5 Histogram of the predicted flood susceptibility for the validation data set (flooding and non-flooding location)

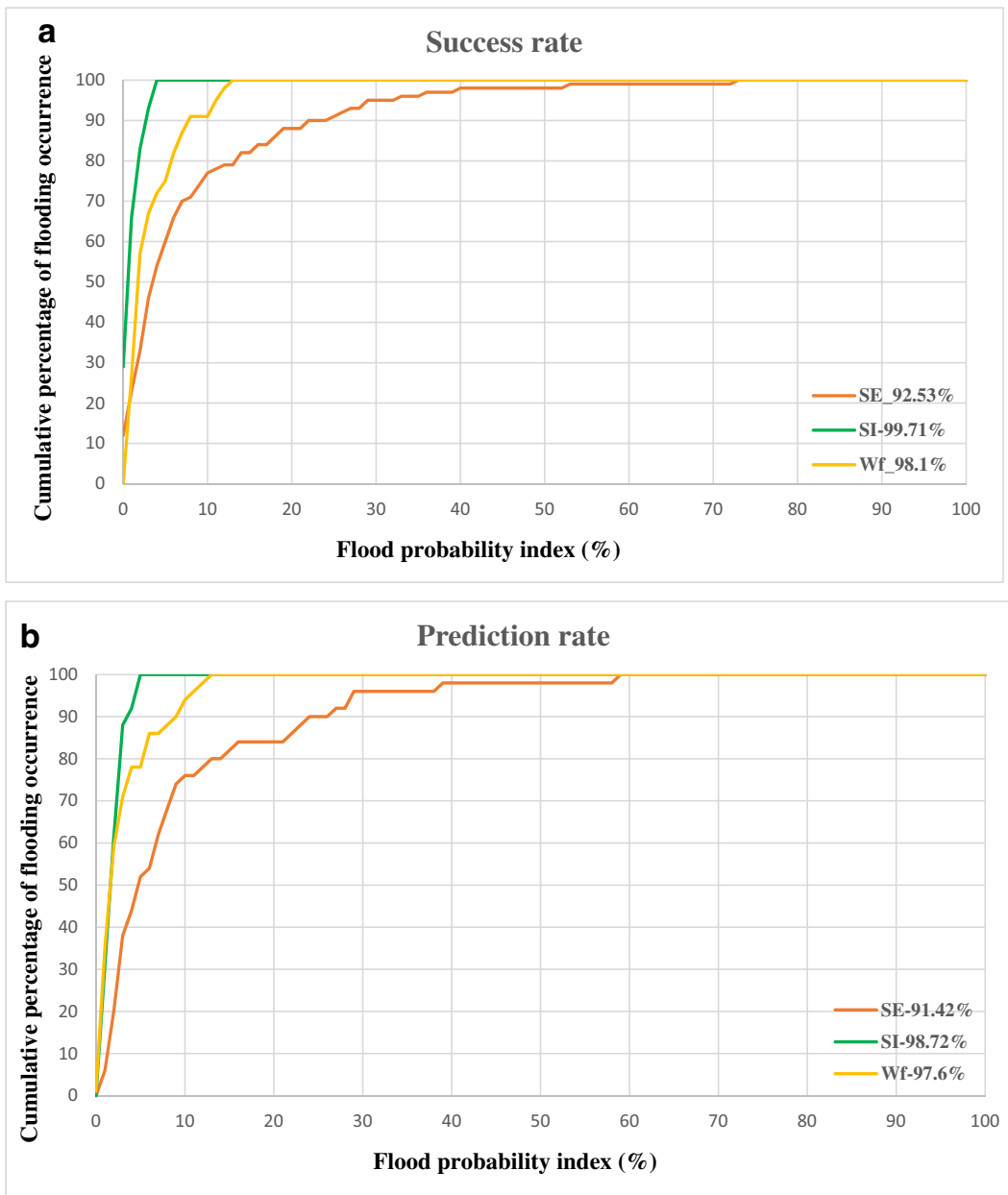


Fig. 6 Validation of FSMs in Haraz Watershed: **a** success rate curve and **b** prediction rate curve

rate, respectively, for SE, SI, and Wf models. The range of AUC is between 0.5 and 1, where one represents the highest accuracy indicating that the model is able to predict natural hazards without any bias (Pradhan 2010a).

For the preparation of success rate and prediction rate, susceptibility maps with 70 and 30% of flooding locations were overlaid and, eventually, the cumulative percentage of flood occurrence (in descending order, from highest to

lowest) was calculated. The success and prediction rate plots were prepared with the x-axis representing the cumulative percentage of flood occurrence and the y-axis representing the flood probability index.

According to the success rate curve and based on the model validation results, the AUC values for SE, SI, and Wf models were respectively measured 0.9253, 0.9971, and 0.981, which were responsible for 92.53, 99.71, and 98.1% accuracy achievement. According to prediction

rate curve and based on the model validation results, AUC values for SE, SI, and Wf models were measured 0.9142, 0.9872, and 0.976, respectively, which were responsible for 91.42, 98.72, and 97.6% accuracy achievement. Yesilnacar (2005) believes that quantitative relationship between the AUC and the accuracy of the model's prediction can be classified into the following classes: weak (0.5–0.6), moderate (0.6–0.7), good (0.7–0.8), very good (0.8–0.9), and excellent (0.9–1). Overall, bivariate statistical models are very suitable for large size of study areas that have a limited data (Zhang et al. 2016) and are very easy to run in a GIS environment (Oh et al. 2011) but have a disadvantage that equal weights are assumed for different effective factors (Pourghasemi and Kerle 2016). Meanwhile, this problem is solved by Shannon's entropy approach. With this interpretation, results of all of the models fall in the excellent category and propose for land use planning and flood management department in the Haraz Watershed, Mazandaran Province.

Conclusion

Flood is one of the world's most hazardous natural events that human societies have faced for decades, while many measures have been done to control and mitigate it. One of the critical steps in this regard is preparation of flood susceptibility maps for future flooding; the most important item for preparation of FSMs is having a reliable and accurate method. The main aims of this study were as follows: (1) floods susceptibility mapping in the Haraz Watershed, Mazandaran Province (due to annual severe flood events) by various methods, namely, FR, SE, SI, and Wf; (2) assessment of models' efficiency in producing flood susceptibility maps; and (3) determination of the most important factors for the occurrence of floods in the study area.

For preparation of flood susceptibility map, initially, the ten causative factors were determined based on the literature review as slope angle, plan curvature, altitude, TWI, SPI, distance from river, rainfall, geology, land use, and NDVI. Then, 211 flood locations (according to field surveys and documentary sources) were identified, of which 70 and 30% were designated, respectively, for the purpose of modeling and validation. Three methods, including SE, SI, and Wf, were used and the relationships between flood events and each of the ten factors

were evaluated. In order to evaluate their performance, the models' efficiencies were compared with that of the FR model, which is one of the popular bivariate statistical techniques in this field.

The histogram and ROC curve methods were used for assessment of the models' ability. In the histogram method, the best model for identification of flooding and non-flooding locations was SI method. By using the AUC, success rate and prediction rate were quantitatively measured for assessment and comparison of FSMs achieved by the four models. The largest area under the success rate curve belonged to the SI (99.71%), followed by the Wf (98.1%) and SE (92.53%).

The results showed that SI method particularly better fitted the training data sets and obtained higher prediction rate by 98.72%. Following the SI method, the AUC values for the Wf and SE methods were measured 98.1 and 92.53%, respectively. The results of four models in the ranking of results were excellent. The results of this research showed that the SI and other models could be regarded as efficient and effective methods for FSMs in GIS environment. Another objective of the current study was determination of the most important causative factor in the Haraz Watershed. Based on the results of the Wf, the order of factors was distance from the river, TWI, and slope angle, while it changed for the SE method to distance from the river, land use, and altitude classes. For either method, the least significant factor was geology.

The results of this study, in addition to utilization as a base map for flood hazard and flood risk mapping, can be used as a contingency plan for the governmental departments of water, disaster management, planning, and others to take appropriate measures to prevent and mitigate floods and their consequent damages in the future.

Acknowledgments The authors would like to thank anonymous reviewers for their helpful comments on the primary version of the manuscript. Also, we are extremely grateful to Prof. Dr. Frederick W. Kutz (associate editor, *Environmental Monitoring and Assessment*) for adding positive comments.

References

- Akgun, A. (2012). A comparison of landslide susceptibility maps produced by logistic regression multi criteria decision and likelihood ratio methods a case study at İzmir Turkey. *Landslides*, 9(1), 93–106.
- Althuwaynee, O. F., Pradhan, B., Park, H. J., & Lee, J. H. (2014). A novel ensemble bivariate statistical evidential belief

- function with knowledge based analytical hierarchy process and multivariate statistical logistic regression for landslide susceptibility mapping. *Catena*, 114, 21–36.
- Asgharizadeh, E., & Nasrolahi, M. (2006). Comparison between fuzzy and Shannon entropy by PROMETHEE model for Iran-Khodro company (Saipa), The 4th International Management Conference. In Persian
- Bahremand, A., De Smedt, F., Corluy, J., Liu, Y., Poorova, J., Velcicka, L., & Kunikova, E. (2007). WetSpa model application for assessing reforestation impacts on floods in Margecany-Hornad Watershed, Slovakia. *Water Resources Management*, 21(8), 1373–1391.
- Bednarik, M., Magulová, B., Matys, M., & Marschalko, M. (2010). Landslide susceptibility assessment of the Kral'ovany–Liptovsky' Mikuláš railway case study. *Physics and Chemistry of the Earth, Parts A/B/C*, 35(3), 162–171.
- Botzen, W., Aerts, J., & van den Bergh, J. (2013). Individual preferences for reducing flood risk to near zero through elevation. *Mitigation Adaptation Strategies Global Change*, 18, 229–244.
- Cevik, E., & Topal, T. (2003). GIS-based landslide susceptibility mapping for a problematic segment of the natural gas pipeline Hendek Turkey. *Environmental Geology*, 44(8), 949–962.
- Chang-Jo, F., & Fabbri, A. G. (2003). Validation of spatial prediction models for landslide hazard mapping. *Natural Hazards*, 30(3), 451–472.
- Chen, Y. R., Yeh, C. H., & Yu, B. (2011). Integrated application of the analytic hierarchy process and the geographic information system for flood risk assessment and flood plain management in Taiwan. *Natural Hazards*, 59(3), 1261–1276.
- Chung, C. F., Fabbri, A. G., & van Western, C. (1995). Multivariate regression analysis for landslide susceptibility zonation. In A. Carrara & F. Guzzetti (Eds.), *Geographical information system in assessing natural hazards* (pp. 107–133). Dordrecht: Kluwer.
- Cloke, H., & Pappenberger, F. (2009). Ensemble flood forecasting: a review. *Journal of Hydrology*, 375(3), 613–626.
- Dai, F. C., & Lee, C. F. (2002). Landslide characteristics and slope instability modeling using GIS, Lantau Island, Hong Kong. *Geomorphology*, 42, 213–228.
- De Moel, H., & Aerts, J. (2011). Effect of uncertainty in land use, damage models and inundation depth on flood damage estimates. *Natural Hazards*, 58, 407–425.
- Elkhrachy, I. (2015). Flash flood hazard mapping using satellite image and GIS tools: a case study of Najran city, Kingdom of Saudi Arabia KSA. *Egyptian Journal of Remote Sensing and Space Science*, 18, 261–278.
- Felicissimo, A., Cuartero, A., Remondo, J., & Quiros, E. (2012). Mapping landslide susceptibility with logistic regression, multiple adaptive regression splines, classification and regression trees, and maximum entropy methods: a comparative study. *Landslides*. doi:10.1007/s10346-012-0320-1.
- Gashaw, W., & Legesse, D. (2011). Flood hazard and risk assessment using GIS and remote sensing in Fogera Woreda, Northwest Ethiopia, *Nile River Basin*. Springer Netherlands 179–206
- Glade, T. (1998). Establishing the frequency and magnitude of landslide-triggering rainstorm events in New Zealand. *Environmental Geology*, 35, 160e–1174.
- Glenn, E., Morino, K., Nagler, P., Murray, R., Pearlstein, S., & Hultine, K. (2012). Roles of saltcedar *Tamarix* spp. and capillary rise in salinizing a non-flooding terrace on a flow-regulated desert river. *Journal of Arid Environment*, 79, 56–65.
- Gokceoglu, C., Sonmez, H., Nefeslioglu, H. A., Duman, T. Y., & Can, T. (2005). The 17 March 2005 Kuzulu landslide (Sivas, Turkey) and landslide-susceptibility map of its near vicinity. *Engineering Geology*, 81, 65–83.
- Hosseinpoor Milaghardan, A., & Abbaspoor, R. A. (2015). Improving landslide prediction results using Shannon entropy theory. *Journal Hazards Sciences*, 1(2), 253–268 (In Persian).
- Jaafari, A., Najafi, A., Pourghasemi, H. R., Rezaeian, J., & Sattarian, A. (2014). GIS-based frequency ratio and index of entropy models for landslide susceptibility assessment in the Caspian forest, northern Iran. *International Journal Environmental Science and Technology*, 11(4), 909–926.
- Jayakrishnan, R., Srinivasan, R., Santhi, C., & Arnold, J. G. (2005). Advances in the application of the SWAT model for water resources management. *Hydrological Processes*, 19, 749–762.
- Jebur, M. N., Pradhan, B., & Tehrany, M. S. (2013). Using ALOS PALSAR derived high resolution DInSAR to detect slow-moving landslides in tropical forest: Cameron Highlands, Malaysia. *Geomatics, Natural Hazard and Risk*, 1–19. doi:10.1080/19475705.2013.860407.
- Jebur, M. N., Pradhan, B., & Tehrany, M. S. (2014). Optimization of landslide causative factors using very high-resolution airborne laser scanning (LiDAR) data at catchment scale. *Remote Sensing of Environment*, 152, 150–165.
- Kazakis, N., Kougiyas, I., & Patsialis, T. (2015). Assessment of flood hazard areas at a regional scale using an index-based approach and analytical hierarchy process: application in Rhodope-Evros region, Greece. *Science of the Total Environment*. doi:10.1016/j.scitotenv.2015.08.055.
- Khosravi, K., Nohani, E., Maroufinia, E., & Pourghasemi, H. R. (2016). A GIS-based flood susceptibility assessment and its mapping in Iran: a comparison between frequency ratio and weights-of-evidence bivariate statistical models with multi-criteria decision-making technique. *Natural Hazards*, 83(2), 1–41.
- Kia, M. B., Pirasteh, S., Pradhan, B., Mahmud, A. R., Sulaiman, W. N. A., & Moradi, A. (2012). An artificial neural network model for flood simulation using GIS: Johor River basin, Malaysia. *Environmental Earth Sciences*, 67, 251–264.
- Konadu, D., & Fosu, C. (2009). Digital elevation models and GIS for watershed modelling and flood prediction—a case study of Accra Ghana, In *Appropriate Technologies for Environmental Protection in the Developing World*. Springer, pp. 325–332.
- Kourgialas, N. N., & Karatzas, G. P. (2011). Flood management and a GIS modelling method to assess flood-hazard areas—a case study. *Hydrological Sciences Journal*, 56(2), 212–225.
- Lee, S., Ryu, J. H., & Kim, I. S. (2007). Landslide susceptibility analysis and its verification using likelihood ratio, logistic regression, and artificial neural network models case study of Youngin, Korea. *Landslides*, 4, 327–338.
- Lee, M.J., Kang, J.E., & Jeon, S. (2012). Application of frequency ratio model and validation for predictive flooded area

- susceptibility mapping using GIS. In: Geoscience and Remote Sensing Symposium (IGARSS), Munich. 895–898
- Li, X. H., Zhang, Q., Shao, M., & Li, Y.L. (2012). A comparison of parameter estimation for distributed hydrological modelling using automatic and manual methods. *Advanced Materials Research*, 356–360, 2372–2375.
- Liu, Y.B., & De Smedt, F. (2004). WetSpa extension, a GIS-based hydrologic model for flood prediction and watershed management. Department of Hydrology and Hydraulic Engineering Vrije Universiteit Brussel. Vrije Universiteit Brussel: Brussels.
- Liu, Y., & De Smedt, F. (2005). Flood modeling for complex terrain using GIS and remote sensed information. *Water Resources Management*, 19, 605–624.
- Massey, D. S., & Nancy, A. D. (1988). The dimensions of residential. *Social Forces*, 67(2), 281–315.
- Meng, Q., Miao, F., Zhen, J., Wang, X., Wang, A., Peng, Y., & Fan, Q. (2015). GIS based landslide susceptibility mapping with logistic regression, analytical hierarchy process, and combined fuzzy and support vector machine methods: a case study from Wolong Giant Panda Natural Reserve, China. *Bulletin Engineering Geology and the Environment*. doi:10.1007/s10064-015-0786-x.
- Mohammady, M., Pourghasemi, H. R., & Pradhan, B. (2012). Landslide susceptibility mapping at Golestan Province, Iran: a comparison between frequency ratio, Dempster–Shafer, and weights-of-evidence models. *Journal of Asian Earth Science*, 61, 221–236.
- Montgomery, D. R. (1994). Road surface drainage, channel initiation, and slope instability. *Water Resources Research*, 30, 1925–1932.
- Naghbi, S. A., Pourghasemi, H. R., Pourtaghi, Z. S., & Rezaei, A. (2014). Groundwater qanat potential mapping using frequency ratio and Shannon’s entropy models in the Moghan Watershed, Iran. *Earth Science Informatics*. doi:10.1007/s12145-014-0145-7.
- Nampak, H., Pradhan, B., & Manap, M. A. (2014). Application of GIS based data driven evidential belief function model to predict groundwater potential zonation. *Journal of Hydrology*, 513, 283–300.
- Oh, H. J., & Lee, S. (2010). Cross-validation of logistic regression model for landslide susceptibility mapping at Geneoung areas, Korea. *Disaster Advance*, 3, 44–55.
- Oh, H. J., & Pradhan, B. (2011). Application of a neuro-fuzzy model to landslide susceptibility mapping for shallow landslides in a tropical hilly area. *Computer and Geosciences*, 37, 1264–1276.
- Oztekun, B., & Topal, T. (2005). GIS-based detachment susceptibility analyses of a cut slope in limestone, Ankara-Turkey. *Environmental Geology*, 49, 124–132.
- Plate, E. J. (2009). HESS opinions: classification of hydrological models for flood management. *Hydrology and Earth System Sciences*, 13, 1939–1951.
- Pourghasemi, H. R., & Kerle, N. (2016). Random forest-evidential belief function based landslide susceptibility assessment in western Mazandaran Province, Iran. *Environmental Earth Sciences*, 75, 185. doi:10.1007/s12665-015-4950-1.
- Pourghasemi, H. R., Mohammadi, M., & Pradhan, B. (2012a). Landslide susceptibility mapping using index of entropy and conditional probability models at Safarood Basin, Iran. *Catena*, 97, 71–84.
- Pourghasemi, H. R., Pradhan, B., & Gokceoglu, C. (2012b). Application of fuzzy logic and analytical hierarchy process (AHP) to landslide susceptibility mapping at Haraz watershed, Iran. *Natural Hazards*. doi:10.1007/s11069-012-0217-2.
- Pourghasemi, H. R., Pradhan, B., & Gokceoglu, C. (2012c). Remote sensing data derived parameters and its use in landslide susceptibility assessment using Shannon’s entropy and GIS. *Applied Mechanics and Materials*, 225, 486–491.
- Pourghasemi, H. R., Moradi, H., & Fatemi Aghda, S. M. (2013). Landslide susceptibility mapping by binary logistic regression, analytical hierarchy process, and statistical index models and assessment of their performances. *Natural Hazards*, 69, 749–779.
- Pradhan, B. (2009). Groundwater potential zonation for basaltic watersheds using satellite remote sensing data and GIS techniques. *Central European Journal of geoscience*, 1(1), 120–129.
- Pradhan, B. (2010a). Flood susceptible mapping and risk area delineation using logistic regression, GIS and remote sensing. *Journal of Spatial Hydrology*, 9, 1–18.
- Pradhan, B. (2010b). Landslide susceptibility mapping of a catchment area using frequency ratio, fuzzy logic and multivariate logistic regression approaches. *Journal of Indian Society Remote Sensing*, 38, 301–320.
- Pradhan, B., & Lee, S. (2010). Delineation of landslide hazard areas on Penang Island, Malaysia, by using frequency ratio, logistic regression, and artificial neural network models. *Environmental Earth Sciences*, 60, 1037–1054.
- Rautela, P., & Lakhera, R. C. (2000). Landslide risk analysis between Giri and Tons Rivers in Himachal Himalaya (India). *International Journal Applied Earth Observation and Geoinformation*, 2, 153–160.
- Sarhadi, A., Soltan, S., & Modarres, R. (2012). Probabilistic flood inundation mapping of ungauged rivers: linking GIS techniques and frequency analysis. *Journal of Hydrology*, 458, 68–86.
- Schanze, J. (2006). Flood risk management –a basic framework. In J. Schanze, E. Zehman, J. Marsalek (Eds.), *Flood Risk Management: Hazards, Vulnerability and Mitigation Measures*, pp. 1–20.
- Sharma, L. P., Patel, N., Ghose, M. K., & Debnath, P. (2013). Synergistic application of fuzzy logic and geo-informatics for landslide vulnerability zonation—a case study in Sikkim Himalayas, India. *Applied Geomatics*. doi:10.1007/s12518-013-0115-7.
- Shirzadi, A., Lee, S., Joo, O. H., & Chapi, K. (2012). A GIS-based logistic regression model in rock-fall susceptibility mapping along a mountainous road: Salavat Abad case study, Kurdistan, Iran. *Natural Hazards*, 64, 1639–1656.
- Tehrany, M. S., Pradhan, B., & Jebur, M. N. (2013). Spatial prediction of flood susceptible areas using rule based decision tree DT and a novel ensemble bivariate and multivariate statistical models in GIS. *Journal of Hydrology*, 504, 69–79.
- Tehrany, M. S., Pradhan, B., & Jebur, M. N. (2014a). Flood susceptibility mapping using a novel ensemble weights-of-evidence and support vector machine models in GIS. *Journal of Hydrology*, 512, 332–343.
- Tehrany, M. S., Lee, M. J., Pradhan, B., Jebur, M. N., & Lee, S. (2014b). Flood susceptibility mapping using integrated bivariate and multivariate statistical models. *Environmental Earth Sciences*, 72(10), 4001–4015.

- Tehrany, M. S., Pradhan, B., & Jebur, M. N. (2015a). Flood susceptibility analysis and its verification using a novel ensemble support vector machine and frequency ratio method. *Stochastic Environmental Research and Risk Assessment*, *29*, 1149–1165.
- Tehrany, M. S., Pradhan, B., Mansor, S. H., & Ahmad, N. (2015b). Flood susceptibility assessment using GIS-based support vector machine model with different kernel types. *Catena*, *125*, 91–101.
- Theil, H. (1972). *Statistical decomposition analysis*. Amsterdam: North-Holland Publishing Company.
- Tien Bui, D., Lofman, O., Revhaug, I., & Dick, O. (2011). Landslide susceptibility analysis in the Hoa Binh province of Vietnam using statistical index and logistic regression. *Natural Hazards*, *59*, 1413–1444.
- Tierney, K. J., Lindell, M. K., & Perry, R. W. (2001). *Facing the unexpected: disaster preparedness and response in the United States*. Washington: Joseph Henry Press.
- van Westen, C. (1997). *Statistical landslide hazard analysis. ILWIS 2.1 for Windows application guide* (pp. 73–84). Enschede: ITC Publication.
- Wan, S. (2009). A spatial decision support system for extracting the core factors and thresholds for landslide susceptibility map. *Engineering Geology*, *108*, 237–251.
- Wu, W., & Sidle, R. C. (1995). A distributed slope stability model for steep forested basins. *Water Resources Research*, *31*, 2097–2110.
- Yalcin, A. (2008). GIS-based landslide susceptibility mapping using analytical hierarchy process and bivariate statistics in Ardesen (Turkey): comparisons of results and confirmations. *Catena*, *72*, 1–12.
- Yalcin, A., Reis, S., Aydinoglu, A. C., & Yomralioglu, T. (2011). A GIS-based comparative study of frequency ratio, analytical hierarchy process, bivariate statistics and logistics regression methods for landslide susceptibility mapping in Trabzon, NE Turkey. *Catena*, *85*(3), 274–287.
- Yang Z, Qiao J, & Zhang X (2010). Regional landslide zonation based on entropy method in three Gorges Area, China. 2010 Seventh International Conference on Fuzzy Systems and Knowledge Discovery (FSKD 2010),1336–1339.
- Yesilnacar, E.K. (2005). The application of computational intelligence to landslide susceptibility mapping in Turkey. Ph.D Thesis Department of Geomatics the University of Melbourne 423 pp.
- Youssef, A. M., Pradhan, B., Jebur, M. N., & El-Harbi, H. M. (2014). Landslide susceptibility mapping using ensemble bivariate and multivariate statistical models in Fayfa area, Saudi Arabi. *Environmental Earth Sciences*, *73*, 3745–3761.
- Youssef, A. M., Pradhan, B., & Sefry, S. A. (2016). Flash flood susceptibility assessment in Jeddah city (Kingdom of Saudi Arabia) using bivariate and multivariate statistical models. *Environmental Earth Sciences*, *75*(12). doi:10.1007/s12665-015-4830-8.
- Yufeng, S., & Fengxiang, J. (2009). Landslide stability analysis based on generalized information entropy. International Conference on Environmental Science and Information Application Technology 83–85.
- Zhang, G., Cai, Y., Zheng, Z., Zhen, J., Liu, Y., & Huang., K. (2016). Integration of the statistical index method and the analytic hierarchy process technique for the assessment of landslide susceptibility in Huizhou, China. *Catena*, *142*, 233–244.